Available online at www.sciencedirect.com

ScienceDirect

Nuclear Physics A 1038 (2023) 122720

NUCLEAR PHYSICS A

www.elsevier.com/locate/nuclphysa

Measurement of alpha-induced reaction cross-sections for ^{nat}Zn with detailed covariance analysis

Mahesh Choudhary [a,*], Aman Sharma [a], Namrata Singh [a], A. Gandhi [a], S. Dasgupta [b], J. Datta [b], K. Katovsky [c], A. Kumar [a,*]

[a] *Department of Physics, Banaras Hindu University, Varanasi-221005, India*

[b] *Analytical Chemistry Division, Bhabha Atomic Research Centre, Variable Energy Cyclotron Centre, Kolkata-700064, India*

[c] *Department of Electrical Power Engineering, Brno University of Technology, Brno-61600, Czech Republic*

Received 25 February 2023; received in revised form 14 June 2023; accepted 6 July 2023
Available online 13 July 2023

Abstract

The production cross-section of ^{68}Ge, ^{69}Ge, ^{65}Zn and ^{67}Ga radioisotopes from alpha-induced nuclear reaction with ^{nat}Zn have been measured using the stacked foil activation technique followed by the off-line γ-ray spectroscopy in the incident alpha energy range 14-37 MeV. The obtained nuclear reaction cross-sections are compared with previous experimental data available in the EXFOR data library, evaluated nuclear data from TENDL-2019 and theoretical results, calculated using TALYS nuclear reaction code. We have also performed the detailed uncertainty analysis for these nuclear reactions and their respective correlation metrics are presented. Since α-induced reactions are important in nuclear medicine and developing the nuclear reaction codes so needful corrections related to the coincidence summing factor and the geometric factor have been considered during the data analysis in the present study.

Keywords: Covariance analysis; Uncertainty quantification; Inter-correlation matrix; Nuclear reactions; Nuclear data analysis

* Corresponding authors.
E-mail addresses: maheshchoudhary921@gmail.com (M. Choudhary), ajaytyagi@bhu.ac.in (A. Kumar).

https://doi.org/10.1016/j.nuclphysa.2023.122720
0375-9474/

1. Introduction

The data on alpha-induced nuclear reaction cross-sections is important for a variety of technological applications including nuclear reaction investigations and the production of medical radionuclides [1,2]. Radioisotopes are being used as therapeutics for a long time and ^{68}Ga is one of such radioisotopes used for PET (Positron Emission Tomography). The production of ^{68}Ga has become more available with the increasing number of medical cyclotrons recently. However, ^{68}Ga has a short half-life of 67.71 minutes and emits positrons with the positron branching ratio 89% accompanied by 1077.34 keV γ-ray. Transport of radioisotopes, like ^{68}Ga, becomes difficult due to their short half-lives. So using ^{68}Ge as a parent to ^{68}Ga is a feasible solution, as it decays to ^{68}Ga with 100% electron capture along with having a relatively longer half-life of 270.95 days. Hence ^{68}Ga/MATHGe generator is an ideal candidate to be used in distant places from the manufacturing site. There are several reactions to produce ^{68}Ge like ^{nat}Zn(α,x), ^{66}Zn(α,2n) etc.

Another prominent medical radioisotope is the ^{67}Ga which is commonly used in nuclear medicine for various types of human tumors and inflammatory lesions [3]. The ^{67}Ga radioisotope has a half-life of 3.26 days and emits γ-ray of 300.22 keV. In this study, α particles bombarded on a natural zinc target with an energy of 37 MeV to produce the above-mentioned medical radioisotopes. Since α-induced reactions are significant in nuclear medicine and developing nuclear reaction codes, precisely estimating the degree of uncertainty propagation from the measured nuclear reaction cross-section data of these nuclear reactions is an important component. Although the EXFOR library [4,5] contains experimental data for these nuclear reactions, none of the data has a complete covariance analysis. Covariance analysis is a method for estimating the uncertainty in a measured quantity by taking cross-correlations into different attributes [6]. In the present work, we have documented detailed covariance analysis of nuclear reactions ^{nat}Zn(α,x)^{68}Ge, ^{nat}Zn(α,x)^{69}Ge, ^{nat}Zn(α,x)^{65}Zn and ^{nat}Zn(α,x)^{67}Ga, by taking the micro correlations between different attributes like decay constant, incident flux, the efficiency of HPGe detector, γ-ray counts, γ-ray intensity and particle number density. We have used TALYS nuclear code [7] for the theoretical calculation of the nuclear reaction cross-section. In the present work, due to the importance of these models, the impacts of six-level density models on the cross-section measurements for the production of the radionuclides ^{68}Ge, ^{69}Ge, ^{65}Zn, and ^{67}Ga through ^{nat}Co(a,x) reactions were examined. The presented excitation functions of these nuclear reactions are compared with the existing experimental data available in the EXFOR library, evaluated nuclear data from TENDL-2019, as well as the theoretical calculation.

The following six components make up the present study, section 2 contains information on the experimental technique and setup, section 3 covers information on the detector's efficiency calibration, section 4 provides information on covariance analysis and theoretical calculations, section 5 takes care of the results and discussion, and section 6 concludes the manuscript.

2. Experimental details

The experiment was carried out at Variable Energy Cyclotron Center (VECC), Kolkata, India using the K-130 cyclotron [8]. In this experiment, helium was used to generate the alpha particles using the penning ionization gauge (PIG) ion source.

We have used the stacked foil activation technique [9–12] followed by the off-line γ-ray spectroscopy to determine the nuclear reaction cross-sections of alpha-induced reactions on ^{nat}Zn in the energy range from the threshold energy of reactions up to 37 MeV. In the stacked foil activa-

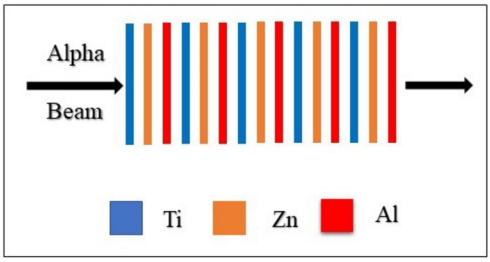

Fig. 1. The schematic presentation of the monitor-target-catcher foil arrangement.

tion method, a particle beam was used to irradiate a stack of multiple thin foils together with a monitor foil. A catcher foil is attached to each target foil to record recoiled radioactive products from the target foil. Al was used as a catcher foil, as it produces only short lived radioactive isotopes in particular energy range, and to reduce gamma attenuation it should has low Z-material.

In this experiment, ^{nat}Zn (10 x 10 mm^2), ^{nat}Al (10 x 10 mm^2) and ^{nat}Ti (10 x 10 mm^2) thin metallic foils were used. The ^{nat}Zn foil was used as target foil, while the ^{nat}Al foil was used as catcher and energy degrader foil. The ^{nat}Ti foil was used as monitor foil and the nuclear reaction ^{nat}Ti(α,x)^{51}Cr was used to calculate incident flux on the target foils. The thickness of thin metallic foils of ^{nat}Zn, ^{nat}Al and ^{nat}Ti were 7.85 $\pm$ 0.05 mg/cm^2, 13.5 $\pm$ 0.08 mg/cm^2 and 1.80 $\pm$ 0.01 mg/cm^2 respectively. In this study we have measured the weight of foil by weighing machine and area by using vernier calliper. To find the thickness of foil in cm we have used the following equation;

$$t = \frac{W(\mathrm{g})}{\rho(\mathrm{g/cm^3})A(\mathrm{cm^2})} \tag{1}$$

Where t is the thickness, W is the weight of the target, A is the area of the foil and the ρ is the density of the target. We have calculated the areal density by using the following formula:

$$t(\mathrm{mg/cm^2}) = t(\mathrm{cm})\rho(\mathrm{mg/cm^3}) \tag{2}$$

Therefor the final uncertainty in the areal density was propagated from uncertainty in the weight of foil and uncertainty in the area. We took a large-size foil, measured the weight and area, and then divided it into 10 equal parts of 10 x 10 mm^2 so that all foils were uniform.

In this work, two different stacks were irradiated to cover the entire excitation function in the incident alpha energy range from the threshold energy up to 37 MeV. We attached an ^{nat}Al foil to a ^{nat}Zn foil in one set of stacks and each stack consisted of five such sets. In each stack, we placed one monitor foil (^{nat}Ti) before every target foil (^{nat}Zn). The details regarding irradiation time, incident energy of alpha particle and beam current for both stacks are given in Table 1. A systematic arrangement of the stacked foils is shown in Fig. 1. In the present experiment two collimators of diameter 8 mm were used and also a Faraday cup was used for current measurement placed after the samples. The charge particle beam from the cyclotron travels a considerable distance after the last quadrupole magnet in the beamline before reaching the target foils. As a result of which, considerable defocusing in the beam can occur. The collimator prevents any stray beam, which does not fall on the target foils to reach the Faraday cup. The collimator thus helps in weeding out error in beam current measurement coming from such defocussed beam. We have used the Stopping and Range of Ions in Matter (SRIM-2008) code to determine the energy loss

Table 1
Irradiation condition and energy range for both stacks in the experiment.

Stack number	Incident energy (MeV)	Energy range (MeV)	Irradiation time (hr)	Current (nA)
Stack 1	37	37-22.2	7	150
Stack 2	32	32-14.5	7	150

in a particular foil [13,14]. This code provides us the information about energy loss of incident ions and range inside the matter.

3. Gamma-ray spectrometry

After irradiation, the activated samples were taken from the experiment hall to the counting room to detect the gamma-ray activity of the samples. After the target holder was safely opened, the monitor foils and the target foils were separated. For gamma-ray activity counting, both the target and the respective catcher foils were wrapped in small thin polythene bags, sealed to prevent from any contamination and placed on perspex plates. Depending on the half-life of the produced radionuclide, counting was started after various cooling intervals from the end of irradiation. In the present study, we have used a high purity germanium detector (HPGe) to detect the gamma-ray activity of the samples. The efficiency of the HPGe detector for different gamma energies was calculated by using a ^{152}Eu point source which has initial activity $A_0 = 3.908 \times 10^4 \pm 197.68$ Bq reported on 17 May 1982. The standard ^{152}Eu point source has a half-life of $T_{1/2} = 13.517 \pm 0.009$ years. The following equation is used to calculate the detection efficiency of the HPGe detector for a source-detector distance of 62.5 mm [15]:

$$\varepsilon_p = \frac{C K_c}{A_0 I_\gamma \Delta t e^{-\lambda t}} \tag{3}$$

In the above equation, ϵ_p represents the efficiency for the point source, λ is the decay constant of ^{152}Eu point source, A_0 represents the known activity of a standard ^{152}Eu point source, C denotes the total number of counts taken in $\Delta t = 10000$ seconds for γ-ray energy with absolute intensity (I_γ), K_C denotes the summing correction factor, and t denotes the cooling time for the point source. A γ-ray spectrum of the irradiated target foil at incident alpha energy 36.32 MeV is shown in Fig. 2. The energy of the incident alpha beam is taken in the middle of every foil.

The samples were of a finite area and the standard source ^{152}Eu was a point source, the efficiency of the point source geometry (ϵ_p) has to be transferred to the efficiency of the sample geometry (ϵ). The Monte Carlo simulation code EFFTRAN [16,17] was used to transfer the efficiency from the point source geometry (ϵ_p) to the sample geometry (ϵ) and calculates the correction factor (K_C) of the coincidence summing effect.

The calculated efficiency value for sample source geometry (ϵ) and point source geometry (ϵ_p) placed at 62.5 mm from the detector are given in Table 3 with the correction factor (K_C). To calculate the efficiency of a particular γ-ray of the product radionuclide, we have used equation (4) which is a fitting function of interpolating the point-wise efficiencies $\epsilon(E_\gamma)$ of the γ-ray energy (E_γ) of the standard source ^{152}Eu [15,18].

$$\varepsilon(E_\gamma) = \varepsilon_c + \varepsilon_o exp(-E_\gamma / E_0) \tag{4}$$

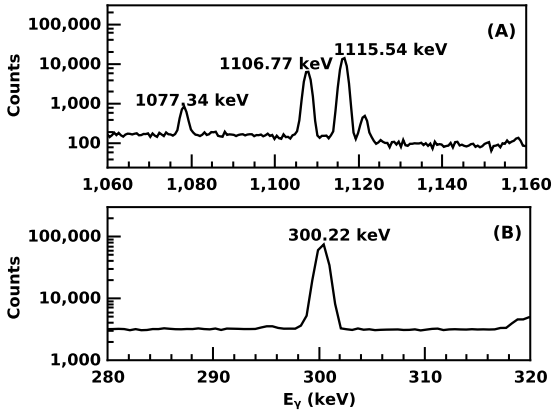

Fig. 2. A γ-ray spectrum of the irradiated target foil at incident alpha energy 36.32 MeV. (a) for radionuclides ^{68}Ge (1077.34 keV), ^{69}Ge (1106.77 keV) and ^{65}Zn (1115.54 keV) (b) for radionuclide ^{67}Ga (300.22 keV).

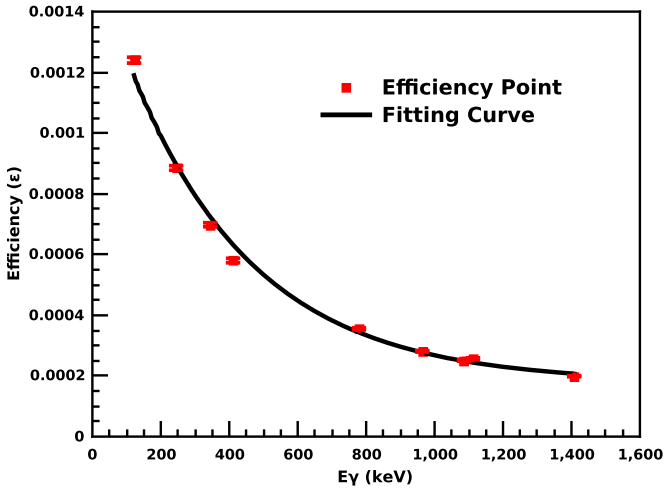

Fig. 3. The HPGe detector efficiency curve for a distance of 62.5 mm between the detector and the source.

Table 2
The value of the detector efficiency (ε) fitting parameters, as well as their uncertainties.

Parameters	Value	Correlation matrix		
ε_c	$1.8 \times 10^{-4} \pm 1.4 \times 10^{-5}$	1		
ε_0	$1.4 \times 10^{-3} \pm 7.4 \times 10^{-5}$	0.522	1	
E_0 (keV)	362 ± 28	-0.892	-0.767	1

Here ε_c, ε_o and E_0 are the detector efficiency (ε) fitting parameters. The value of these fitting parameters, uncertainties and their correlation matrix are given in Table 2. The efficiency curve of the HPGe detector is shown in Fig. 3.

Table 3
The HPGe detector's efficiency for both sample (ε) and point source (ε_p) geometries at different γ-ray energies with their γ-ray intensities and coincidence summing correction factor (K_c).

E_γ (keV)	I_γ (%)	Counts (C)	K_c	ε_p	ε
121.78	28.53 ± 0.16	376755 ± 640	1.02	0.00138	0.00124 ± 0.0000096
244.69	7.55 ± 0.04	70512 ± 296	1.03	0.00098	0.00088 ± 0.0000075
344.27	26.59 ± 0.2	197352 ± 454	1.02	0.00077	0.00069 ± 0.0000065
411.11	2.24 ± 0.01	13571 ± 137	1.03	0.00064	0.00058 ± 0.0000074
778.9	12.93 ± 0.08	48579 ± 288	1.02	0.00039	0.00035 ± 0.0000035
964.05	14.51 ± 0.07	43529 ± 231	1.01	0.00031	0.00028 ± 0.0000025
1085.83	10.11 ± 0.05	27617 ± 177	0.99	0.00028	0.00025 ± 0.0000024
1112.94	13.67 ± 0.08	37596 ± 203	1.0	0.00028	0.00026 ± 0.0000024
1408.01	20.87 ± 0.09	44423 ± 218	1.0	0.00022	0.00019 ± 0.0000016

Table 4
Nuclear reactions and details about other parameters of the radionuclides generated through ^{nat}Zn(α,x) reactions.

Radionuclide	Half-life ($t_{1/2}$)	Decay mode (%)	E_γ (keV)	I_γ (%)	Reaction	Q-value (MeV)
^{65}Zn	243.93 ± 0.09 days	$ec + \beta^+$(100)	1115.54	50.04 ± 0.1	^{64}Zn(α, He^3)	-12.59
					^{64}Zn(α, n+2p)	-20.31
					^{64}Zn(α, p+d)	-18.09
					^{66}Zn(α, a+n)	-11.05
^{67}Ga	3.2617 ± 0.0005 days	ec (100)	300.22	16.64 ± 0.12	^{64}Zn(α,p)	-3.99
					^{66}Zn(α,t)	-14.55
					^{66}Zn(α,2n+p)	-23.03
					^{67}Zn(α,3n+p)	-30.08
^{68}Ge	270.93 ± 0.13 days	ec (100)	-	-	^{64}Zn(α,γ)	3.39
					^{66}Zn(α,2n)	-15.64
					^{67}Zn(α,3n)	-22.69
					^{68}Zn(α,4n)	-32.88
^{68}Ga	67.71 ± 0.08 min	$ec + \beta^+$(100)	1077.34	3.22 ± 0.03	^{68}Ge (ec)	
^{69}Ge	39.05 ± 0.1 h	$ec + \beta^+$(100)	1106.77	36.0 ± 0.4	^{66}Zn(α,n)	-7.44
					^{67}Zn(α,2n)	-14.49
					^{68}Zn(α,3n)	-24.69

4. Data analysis

4.1. Estimation of the reaction cross section

In the present study, the following activation formula was used to calculate the cross-sections of the nuclear reactions;

$$\sigma_s = \sigma_m \frac{\lambda_s C_s I_m \varepsilon_m N_m (1 - e^{-\lambda_m t_{im}})(e^{-\lambda_m t_{cm}})(1 - e^{-\lambda_m t_{am}})}{\lambda_m C_m I_s \varepsilon_s N_s (1 - e^{-\lambda_s t_{is}})(e^{-\lambda_s t_{cm}})(1 - e^{-\lambda_s t_{as}})} \tag{5}$$

Here σ_s, σ_m are the cross-sections of the sample and monitor nuclear reactions, λ_s, λ_m are the decay constants for the sample and monitor nuclear reactions, C_s, C_m are the peak area counts for the sample and monitor foils, I_s, I_m represent the gamma-ray intensities of the produced radioisotopes from the sample and monitor foils, ε_s, ε_m are the detector efficiencies for the sample

and monitor nuclear reactions and N_s, N_m are the particle number densities for the sample and monitor foils. In equation (5), $(t_i)_{s,m}$, $(t_c)_{s,m}$ and $(t_a)_{s,m}$ are the irradiation time, cooling time and counting time for the sample and monitor foils respectively.

To determine the uncertainty of the measured nuclear reaction cross-section, the uncertainty in the parameters contributing to the cross-section is taken into account such as monitor cross-section, detector efficiency, gamma-ray intensity, the particle number density in target, peak area counts and decay constant. The details regarding nuclear reactions, half-life, decay data and Q-value of the reactions are given in the Table 4.

4.2. Covariance analysis

The cross-correlation between several measured values can be used to explain the detailed uncertainty in covariance analysis. The covariance matrix (I_σ) of the cross-section can be represented as [19–21];

$$I_\sigma = S_x C_x S_x^T \tag{6}$$

In the above equation, I_σ represents the covariance matrix of the measured nuclear reaction cross-sections of order r × r and C_x matrix of order m × m, represents the semi covariance matrix of different variables in the cross-section formula (equation (5)) i.e. peak area counts (C_γ), detector efficiency $\varepsilon(E_\gamma)$, flux (ϕ), decay constant (λ), γ-ray intensity (I_γ), particle number density in the target (N_t). Here, S_x represents the sensitivity matrix with the corresponding element (j, k);

$$S_{xjk} = \frac{\partial \sigma_j}{\partial x_k};\ (j = 1, 2, 3, ...r;\ k = 1, 2, 3, ...m) \tag{7}$$

Here, the total number of the measured cross-sections for a nuclear reaction is equal to r and the total number of variables in the cross-section formula is equal to m. If two variables x_k and x_l (k, l = 1, 2, 3,.....m) are required in the calculation of the cross-sections, then we can write covariance matrix (C_x) of these variables as follows [22–24];

$$C_x(x_k, x_l) = Cor(x_k, x_l)(\Delta x_k \Delta x_l) \tag{8}$$

In the above equation, the term $Cor(x_k, x_l)$ represents the correlation coefficient between two attributes x_k, x_l and it has a value in the range of 0 to 1. If k=l then the value of the term $Cor(x_k, x_l)$ is equal to 1, in which case these two variables x_k, x_l are fully correlated. The interpolated efficiency, error and correlation matrix of the γ-ray for the nuclear reactions of the sample and monitor are given in Table 5.

The percentage uncertainties of the different parameters contributing to the uncertainties of the sample nuclear reaction cross-sections are given in Table 6. The calculated spread in the incident alpha beam energy for each energy point is given in Tables 7–10 and shown in Figs. 4–7.

4.3. Theoretical calculations

We have used the statistical nuclear model code TALYS-1.9 [25] for the theoretical calculations of the reactions ^{nat}Zn(α,x)^{68}Ge, ^{nat}Zn(α,x)^{69}Ge, ^{nat}Zn(α,x)^{65}Zn and ^{nat}Zn(α,x)^{67}Ga. The TALYS is a Fortran-based nuclear reaction model code which is used to calculate different physical observables related to nuclear reactions. This nuclear code is based on the Hauser–Fesbach statistical model and it contains distinct choices for level density and optical model parameters

Table 5
The Interpolated efficiency, error and correlation matrix of the γ-ray for the nuclear reactions of the sample and monitor.

Reaction	E_γ (keV)	Efficiency (ϵ)	Error ($\Delta\epsilon$)	Correlation matrix	
^{nat}Ti(α,x)^{51}Cr	320.08	0.00076	0.0000176	1	
^{nat}Zn(α,x)^{65}Zn	1115.50	0.00024	0.0000055	0.0953	1
^{nat}Ti(α,x)^{51}Cr	320.08	0.00076	0.0000176	1	
^{nat}Zn(α,x)^{68}Ge	1077.30	0.00025	0.0000056	0.174	1
^{nat}Ti(α,x)^{51}Cr	320.08	0.00076	0.0000176	1	
^{nat}Zn(α,x)^{69}Ge	1106.77	0.00024	0.0000055	0.114	1
^{nat}Ti(α,x)^{51}Cr	320.08	0.00076	0.0000176	1	
^{nat}Zn(α,x)^{67}Ga	300.22	0.00079	0.0000182	0.994	1

Table 6
The percentage uncertainties of the different parameters contributing to the uncertainties of the sample nuclear reaction cross-sections.

Parameters	^{nat}Zn(α,x)^{65}Zn	^{nat}Zn(α,x)^{68}	^{nat}Zn(α,x)^{69}Ge	^{nat}Zn(α,x)^{67}Ga
x_i	Δx_i (%)	Δx_i (%)	Δx_i (%)	Δx_i (%)
σ_m	4-6	4-6	4-7	4-7
C_s	0.5-5	0.5-4	0.5-2	0.5-1.5
C_m	0.5-1	0.5-1	0.5-1	0.5-1
λ_m	0.01	0.01	0.01	0.01
λ_s	0.04	0.05	0.26	0.02
I_m	0.1	0.1	0.1	0.1
I_S	0.2	0.93	1.11	0.72
N_m	0.56	0.56	0.56	0.56
N_s	0.67	0.67	0.67	0.67
ϵ_m	2.31	2.31	2.31	2.31
ϵ_s	2.25	2.24	2.25	2.30

[26]. In this nuclear code, we can do calculations for nuclear reactions having projectiles such as photons, neutrons, protons, tritons, deuterons, ^{3}He- and alpha-particles and target nuclides with masses of 12 and larger in the 1 keV - 200 MeV energy range. The TALYS have six different level density models. The ldmodel-1 is related to the constant temperature and the Fermi gas model, ldmodel-2 is related to the back-shifted Fermi gas model, ldmodel-3 is related to the generalized superfluid model, ldmodel-4 is from the Goriely table (Skyrme Force), ldmodel-5 is from Hilaire's combinatorial tables (Skyrem force) and ldmodel-6 is from Hilaire's combinatorial tables (temperature-dependent HFB, Gogny force). Among these six level density models ldmodel-1, 2, 3 are phenomenological level density models and ldmodel-4, 5, 6 are microscopic level density models [27–32]. In the present work we have used all these six level density models and the results of the theoretical calculations were compared with the experimentally obtained nuclear reaction cross-sections.

5. Results and discussion

We have reported reaction cross-sections, uncertainties and a covariance matrix of ^{nat}Zn(α,x) nuclear reactions for the projectile energy range from the corresponding threshold energy for

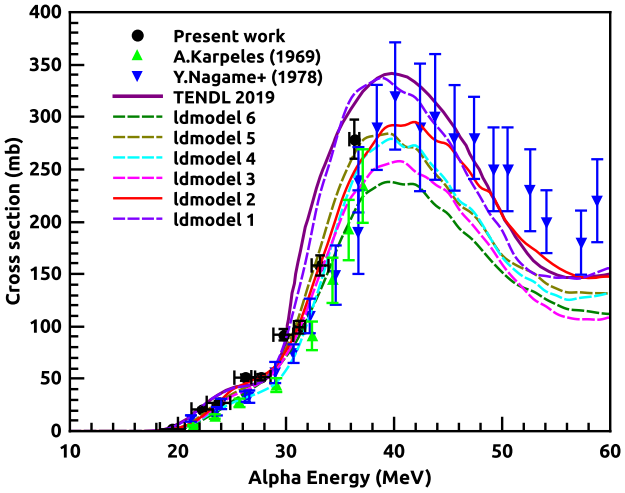

Fig. 4. Cross sections for ^{nat}Zn(α,x)^{65}Zn reaction from this study in comparison of the available experimental data from EXFOR and theoretical calculation from TALYS. (For interpretation of the colours in the figure(s), the reader is referred to the web version of this article.)

each contributing reaction up to 37 MeV. In the present work, the measured nuclear reaction cross-sections compared to the theoretical prediction from the TALYS nuclear reaction code, evaluated data from TENDL-2019 and the existing experimental data from EXFOR. The excitation functions of nuclear reactions are shown in Figs. 4–7 and measured reaction cross-sections with their correlation matrices are presented in Tables 7–10.

5.1. Production cross-section of ^{65}Zn

The measured nuclear reaction cross-section value for the ^{nat}Zn(α,x)^{65}Zn nuclear reaction is presented in Fig. 4 along with the theoretical excitation function from the TALYS code, evaluated nuclear data from TENDL-2019 and previously calculated cross-sections available on the EXFOR. The cross-sections for the ^{nat}Zn(α,x)^{65}Zn nuclear reaction were estimated using a γ-ray with an energy of 1115.54 keV and intensity of 50.04% that arises from the decay of ^{65}Zn radionuclide. The calculated experimental results for ^{nat}Zn(α,x)^{65}Zn reaction are in good agreement with the existing reaction data given by A. Karpeles and Y. Nagame et al. [33,34], as shown in Fig. 4. The theoretical results from ldmodel-2 (represented in red colour by a solid line) follow the trend of excitation function of this nuclear reaction. There is a good agreement between evaluated nuclear data from TENDL-2019 and the theoretical result from ldmodel-1 for the nuclear reaction ^{nat}Zn(α,x)^{65}Zn. The obtained reaction cross-sections, as well as their uncertainties and correlation matrix for the reaction ^{nat}Zn(α,x)^{65}Zn are given in Table 7.

5.2. Production cross-section of ^{68}Ge

In the present work, the measured nuclear reaction cross-section value for the ^{nat}Zn(α,x)^{68}Ge nuclear reaction is presented in Fig. 5 along with the theoretical excitation function from the TALYS code, evaluated nuclear data from TENDL-2019 and previously calculated cross-sections available on the EXFOR. The cross-sections for the ^{nat}Zn(α,x)^{68}Ge nuclear reaction were esti-

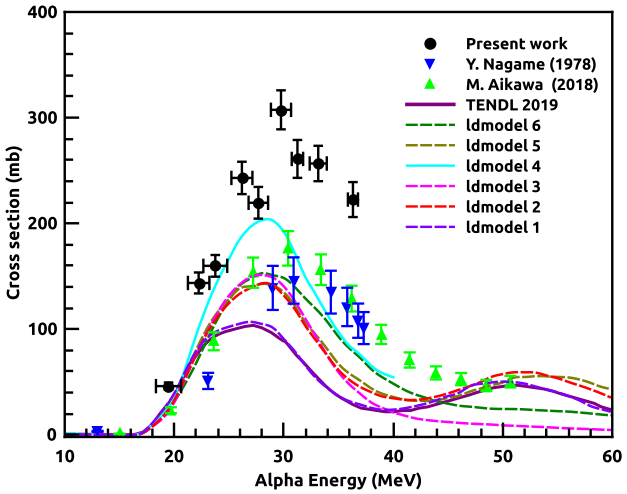

Fig. 5. Cross sections for ^{nat}Zn(α,x)^{68}Ge reaction from this study in comparison of the available experimental data from EXFOR and theoretical calculation from TALYS.

Table 7
The calculated reaction cross-section, uncertainty and correlation matrix of the nuclear reaction ^{nat}Zn(α,x)^{65}Zn.

E_α (MeV)	Cross-section (mb) ($\sigma \pm \triangle\sigma$)	Correlation matrix								
19.47 ± 1.15	1.78 ± 0.14	1								
22.23 ± 0.98	20.74 ± 1.41	0.193	1							
23.75 ± 1.09	27.01 ± 1.78	0.199	0.228	1						
26.18 ± 0.96	51.10 ± 2.99	0.224	0.257	0.265	1					
27.68 ± 0.89	51.49 ± 3.0	0.225	0.258	0.267	0.300	1				
29.75 ± 0.92	92.09 ± 5.44	0.222	0.255	0.263	0.296	0.297	1			
31.25 ± 0.52	99.27 ± 6.09	0.214	0.245	0.253	0.285	0.286	0.283	1		
33.15 ± 0.78	158.20 ± 9.63	0.216	0.247	0.255	0.287	0.288	0.285	0.274	1	
36.32 ± 0.46	278.78 ± 18.68	0.196	0.224	0.232	0.261	0.262	0.259	0.249	0.251	1

Table 8
The calculated reaction cross-section, uncertainty and correlation matrix of the nuclear reaction ^{nat}Zn(α,x)^{68}Ge.

E_α (MeV)	Cross-section (mb) ($\sigma \pm \triangle\sigma$)	Correlation matrix								
19.47 ± 1.15	34.12 ± 2.49	1								
22.23 ± 0.98	122.77 ± 8.31	0.206	1							
23.75 ± 1.09	137.44 ± 8.61	0.222	0.240	1						
26.18 ± 0.96	219.70 ± 13.51	0.227	0.245	0.264	1					
27.68 ± 0.89	206.37 ± 13.82	0.208	0.225	0.243	0.247	1				
29.75 ± 0.92	294.34 ± 17.21	0.238	0.257	0.278	0.283	0.260	1			
31.25 ± 0.52	260.66 ± 17.56	0.207	0.223	0.241	0.246	0.226	0.258	1		
33.15 ± 0.78	256.54 ± 16.37	0.218	0.236	0.255	0.259	0.238	0.273	0.237	1	
36.32 ± 0.46	222.56 ± 16.25	0.191	0.206	0.222	0.226	0.208	0.238	0.207	0.218	1

Table 9
The calculated reaction cross-section, uncertainty and correlation matrix of the nuclear reaction ^{nat}Zn(α,x)^{69}Ge.

E_α (MeV)	Cross-section (mb) ($\sigma \pm \triangle\sigma$)	Correlation matrix									
14.47 ± 1.17	232.55 ± 17.26	1									
19.48 ± 1.15	257.65 ± 16.64	0.235	1								
22.23 ± 0.98	291.90 ± 17.77	0.250	0.288	1							
23.75 ± 1.09	171.25 ± 9.98	0.261	0.300	0.319	1						
26.18 ± 0.96	119.37 ± 6.94	0.262	0.301	0.320	0.334	1					
27.68 ± 0.89	85.28 ± 5.03	0.258	0.297	0.315	0.329	0.330	1				
29.75 ± 0.92	82.20 ± 4.91	0.254	0.293	0.311	0.325	0.326	0.321	1			
31.25 ± 0.52	75.20 ± 4.67	0.245	0.281	0.299	0.312	0.313	0.308	0.304	1		
33.15 ± 0.78	77.23 ± 4.79	0.245	0.282	0.300	0.313	0.314	0.309	0.306	0.294	1	
36.32 ± 0.46	105.50 ± 7.17	0.224	0.258	0.274	0.286	0.287	0.282	0.279	0.268	0.269	1

mated using a γ-ray with an energy of 1077.34 keV and intensity of 3.22% that arises from the decay of ^{68}Ga radionuclide. The radioisotope ^{68}Ge decays to ^{68}Ga with 100% electron capture. The measured experimental results for the ^{nat}Zn(α,x)^{68}Ge reaction are higher than the existing experimental data given by Y. Nagame et al. and M. Alkawa et al. [34,35], as shown in Fig. 5. The theoretical results from ldmodel-4 (represented in cyan colour by a solid line) partially follow the trend of present experimental data. We have used the optical model potential for alpha projectile with the level density model 4 to reduce the discrepancy between the theoretical predictions and the experimental results. We have used the Woods–Saxon shape adjustable parameter (equal to 1.3) with ldmodel 4 in the TALYS nuclear code for the theoretical calculation of this nuclear reaction. The theoretical results from ldmodel-4 are in good agreement with measured experimental results for this reaction in the energy range 19-28 MeV and results from the ldmodel-4 are lower then measured experimental results in the energy range 29-37 MeV. It is clear from Fig. 5 that the data evaluated by TENDL-2019 do not follow the experimental data obtained by us as well as the data reported by Y. Nagame et al. and M. Alkawa et al. There is a good agreement between evaluated nuclear data from TENDL-2019 and the theoretical result from ldmodel-1 for the nuclear reaction ^{nat}Zn(α,x)^{68}Ge. The obtained reaction cross-sections, as well as their uncertainties and correlation matrix for the nuclear reaction ^{nat}Zn(α,x)^{68}Ge are given in Table 8.

5.3. Production cross-section of ^{69}Ge

In the present work, the measured nuclear reaction cross-section value for the ^{nat}Zn(α,x)^{69}Ge nuclear reaction is presented in Fig. 6 along with the theoretical excitation function from the TALYS code and previously calculated cross-sections available on the EXFOR. The cross-sections for the ^{nat}Zn(α,x)^{69}Ge nuclear reaction were estimated using a γ-ray with an energy of 1106.77 keV and intensity of 36% that arises from the decay of ^{69}Ge radionuclide. The calculated experimental results for ^{nat}Zn(α,x)^{69}Ge reaction partially follow the trend of existing experimental data given by Y. Nagame et al. and M. Aikawa et al. [34,35], as shown in Fig. 6. The measured experimental results for this reaction are higher than the existing experimental data in the energy range 14-20 MeV and are in good agreement with the existing experimental data in the energy range 21-37 MeV. The theoretical results from ldmodel-6 are in good agreement with the measured experimental results for this reaction. We have used optical model potential for alpha projectile with the ldmodel 6 to reduce the discrepancy between the theoretical predictions and the experimental results. We have used the Woods-Saxon shape adjustable parameters (equal

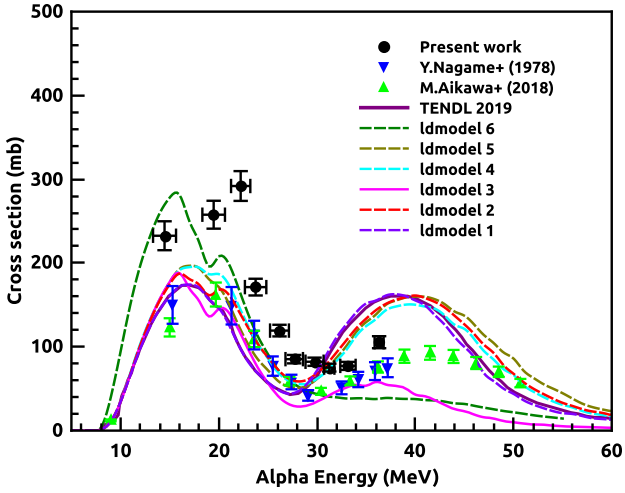

Fig. 6. Cross sections for ^{nat}Zn(α,x)^{69}Ge reaction from this study in comparison of the available experimental data from EXFOR and theoretical calculation from TALYS.

Table 10
The calculated reaction cross-section, uncertainty and correlation matrix of the nuclear reaction ^{nat}Zn(α,x)^{67}Ga.

E_α (MeV)	Cross-section (mb) ($\sigma \pm \triangle\sigma$)	Correlation matrix									
14.47 ± 1.17	486.98 ± 32.87	1									
19.48 ± 1.15	617.18 ± 34.74	0.036	1								
22.23 ± 0.98	536.43 ± 28.08	0.038	0.046	1							
23.75 ± 1.09	392.25 ± 21.78	0.036	0.044	0.047	1						
26.18 ± 0.96	214.52 ± 10.54	0.041	0.049	0.053	0.050	1					
27.68 ± 0.89	168.23 ± 12.57	0.027	0.032	0.035	0.033	0.037	1				
29.75 ± 0.92	97.09 ± 6.47	0.030	0.036	0.039	0.037	0.042	0.027	1			
31.25 ± 0.52	95.08 ± 8.99	0.021	0.026	0.027	0.026	0.029	0.019	0.022	1		
33.15 ± 0.78	67.37 ± 6.54	0.021	0.025	0.027	0.025	0.029	0.019	0.021	0.015	1	
36.32 ± 0.46	101.06 ± 7.29	0.028	0.034	0.036	0.034	0.038	0.025	0.028	0.020	0.019	1

to 1.3) and the volume central potential adjustable parameters (equal to 1.12, 1.18 and 1.89) with ldmodel 6 in the TALYS nuclear reaction code for theoretical calculation of this nuclear reaction. It is clear from Fig. 6 that the data evaluated by TENDL-2019 do not follow the experimental data obtained by us as well as the data reported by Y. Nagame et al. and M. Alkawa et al. There is a good agreement between evaluated nuclear data from TENDL-2019 and the theoretical result from ldmodel-1 for the nuclear reaction ^{nat}Zn(α,x)^{69}Ge. The obtained reaction cross-sections, as well as their uncertainties and correlation matrix for the nuclear reaction ^{nat}Zn(α,x)^{69}Ge are given in Table 9.

5.4. Production cross-section of ^{67}Ga

In our work, the measured nuclear reaction cross-section value for the ^{nat}Zn(α,x)^{67}Ga nuclear reaction is presented in Fig. 7 along with the theoretical excitation function from the TALYS code and previously calculated cross-sections available on the EXFOR. The cross-sections for

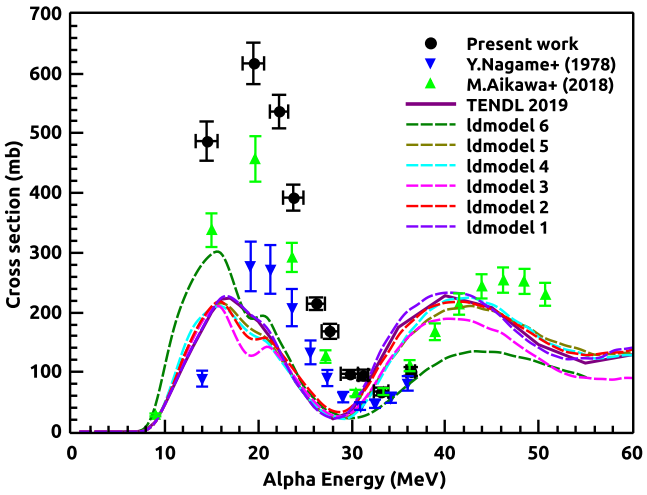

Fig. 7. Cross sections for ^{nat}Zn(α,x)^{67}Ga reaction from this study in comparison of the available experimental data from EXFOR and theoretical calculation from TALYS.

the ^{nat}Zn(α,x)^{67}Ga nuclear reaction were estimated using a γ-ray with an energy of 300.22 keV and intensity of 16.64% that arises from the decay of ^{67}Ga radionuclide.

The measured experimental results for ^{nat}Zn(α,x)^{67}Ga reaction partially follow the trend of existing experimental data given by Y. Nagame et al. and M. Aikawa et al. [34,35], as shown in Fig. 7. The measured experimental results for this reaction are higher than the existing experimental data in the energy range 14-20 MeV and are in good agreement with the existing experimental data in the energy range 21-37 MeV. We have used optical model potential for alpha projectile with the ldmodel 6 to reduce the discrepancy between the theoretical predictions and the experimental results. We used the Woods-Saxon shape adjustable parameters (equal to 1.3) and the volume central potential adjustable parameters (equal to 1.12, 1.18 and 1.89) with ldmodel 6 in the TALYS nuclear reaction code for theoretical calculation of this nuclear reaction. The theoretical results are slightly lower than the experimental results of this nuclear reaction in the energy range 10-30 MeV. It is clear from Fig. 7 that the data evaluated by TENDL-2019 do not follow the experimental data obtained by us as well as the data reported by Y. Nagame et al. and M. Aikawa et al. There is a good agreement between evaluated nuclear data from TENDL-2019 and the theoretical result from ldmodel-1 for the nuclear reaction ^{nat}Zn(α,x)^{67}Ga. The obtained reaction cross-sections, as well as their uncertainties and correlation matrix for the nuclear reaction ^{nat}Zn(α,x)^{67}Ga are given in Table 10.

6. Conclusion

In the present study, we have measured the cross-sections for ^{nat}Zn(α,x)^{68}Ge, ^{nat}Zn(α,x)^{69}Ge, ^{nat}Zn(α,x)^{65}Zn and ^{nat}Zn(α,x)^{67}Ga nuclear reactions using the stack foil activation technique for the projectile energy range 14-37 MeV, a complete covariance analysis has also been performed. The detailed uncertainty analysis for above mentioned reactions, as well as their accompanying correlation matrix, is documented. The optical model parameters are not appropriate for the alpha-induced nuclear reaction with different targets. We have used the Woods-Saxon shape adjustable parameters (equal to 1.3) and the volume central potential adjustable parameters

(equal to 1.12, 1.18 and 1.89) with different ldmodels in the TALYS nuclear reaction code for theoretical calculation of above-mentioned nuclear reactions. The measured cross-sections for ^{nat}Zn(α,x)^{65}Zn nuclear reaction are in good agreement with existing experimental data from the EXFOR, the measured cross-sections for ^{nat}Zn(α,x)^{68}Ge, ^{nat}Zn(α,x)^{69}Ge and ^{nat}Zn(α,x)^{67}Ga nuclear reactions partially follow the existing experimental data. The ldmodel-4 provides the most accurate theoretical results for ^{nat}Zn(α,x)^{68}Ge, ldmodel-6 provides the most accurate theoretical results for ^{nat}Zn(α,x)^{69}Ge nuclear reaction and the ldmodel-2 provide the most accurate theoretical results for ^{nat}Zn(α,x)^{65}Zn nuclear reaction. The theoretical results of ldmodel-4 follow the trend of the excitation function above 30 MeV energy for the ^{nat}Zn(α,x)^{67}Ga nuclear reaction. The discrepancy between the experimental cross-section and the theoretical predictions can be reduced if we choose the correct set of optical model potentials with a level density model for the alpha-induced nuclear reaction. The ldmodel-2 is based on the back-shifted Fermi gas model, the ldmodel-4 based on Skyrme force from Goriely's tables while the ldmodel-6 relates to Hilaire's combinatorial tables (temperature-dependent HFB, Gogni force). The evaluated data from the TENDL-2019 are consistent with the theoretical results obtained from the ldmodel-1. It looks from the present study that the evaluation results obtained from TENDL-2019 need corrections.

CRediT authorship contribution statement

Mahesh Choudhary (first author), involved in writing the manuscript, performing the experiment for the present study and analysed the experimental data. **A. Kumar (corresponding author)**, played an important role in shaping the manuscript. All the work presented in this manuscript was done under the supervision of A. Kumar. He played a pivotal role in writing and editing the manuscript. Additionally, A. Kumar provided critical supervision during the experiment, which ensured its successful execution. We would also like to acknowledge the contributions of our co-authors, namely Aman Sharma, Namrata Singh, A. Gandhi, S. Dasgupta, J. Datta, and K. Katovsky. Their collective efforts played an important role in the successful execution of the experiment for the present study.

Declaration of competing interest

The authors declare that they have no known competing financial interests or personal relationships that could have appeared to influence the work reported in this paper.

Data availability

Data will be made available on request.

Acknowledgements

The author (Mahesh Choudhary) is thankful for financial support in the form of Senior Research Fellowships from the Council of Scientific and Industrial Research (CSIR), Government of India, (File No 09/013(882)/2019-EMR-1). The SERB, DST, Government of India [Grant No. CRG/2019/000360], IUAC-UGC, Government of India (Sanction No. IUAC/XIII.7 /UFR-71353) and Institutions of Eminence (IoE) BHU [Grant No. 6031] are also gratefully acknowledged by one of the authors (A. Kumar).

We acknowledge the kind support provided by Prof. Chandana Bhattacharya, Head, Experimental Nuclear Physics Division, VECC, Kolkata and Prof. A. K. Tyagi, Director, Chemistry Group, BARC, Mumbai towards the successful execution of the experiment. We would also like to express our gratitude to VECC Cyclotron (K-130) staff for providing us with high-quality beams throughout the experiment.

References

[1] B. Mukhopadhyay, K. Mukhopadhyay, J. Nucl. Med. Radiat. Ther. 2 (2) (2011) 1000115.
[2] A.A. Alharbi, et al., in: Radioisotopes-Applications in Bio-Medical Science, IntechOpen, 2011.
[3] R. Avagyan, et al., Univers. J. Math. Appl. 2 (7) (2014) 221.
[4] N. Otuka, et al., Nucl. Data Sheets 120 (2014) 272.
[5] IAEA-EXFOR Experimental nuclear reaction database, https://www-nds.iaea.org/exfor (Data retrieved on January 2023).
[6] M. Choudhary, et al., Eur. Phys. J. A 58 (2022) 95.
[7] A.J. Koning, S. Hilaire, M.C. Duijvestijn, TALYS-1.0, in: O. Bersillon, F. Gunsing, E. Bauge, R. Jacqmin, S. Leray (Eds.), Proceedings of the International Conference on Nuclear Data for Science and Technology, April 22-27, 2007, Nice, France, EDP Sciences, 2008, p. 211.
[8] A. Goswami, et al., Pramana 93 (2019) 1–13.
[9] M.S. Uddin, K.S. Kim, M. Nadeem, S. Sudar, G.N. Kim, Eur. Phys. J. A 53 (5) (2017) 1–10.
[10] S. Takacs, M.P. Takacs, A. Hermanne, F. Tarkanyi, R.A. Rebeles, Nucl. Instrum. Methods Phys. Res., Sect. B, Beam Interact. Mater. Atoms 297 (2013) 44–57.
[11] S. Takacs, M.P. Takacs, A. Hermanne, F. Tarkanyi, R.A. Rebeles, Nucl. Instrum. Methods Phys. Res., Sect. B, Beam Interact. Mater. Atoms 278 (2012) 93–105.
[12] T. Siiskonen, J. Huikari, T. Haavisto, J. Bergman, S.J. Heselius, J.O. Lill, T. Lonnroth, K. Perajarvi, Appl. Radiat. Isot. 67 (11) (2009) 2037–2039.
[13] J.F. Ziegler, J.P. Biersack, M.D. Ziegler, SRIM-The Stopping and Range of Ions in Matter (SRIM Co., 2008), http://www.SRIM.org, 2018.
[14] Peter Sigmund, Schinner Andreas, Nucl. Instrum. Methods Phys. Res., Sect. B, Beam Interact. Mater. Atoms 410 (2017) 78–87.
[15] L.R.M. Punte, B. Lalremruata, N. Otuka, S.V. Suryanarayana, Y. Iwamoto, R. Pachuau, B. Satheesh, H.H. Thanga, L.S. Danu, V.V. Desai, L.R. Hlondo, S. Kailas, S. Ganesan, B.K. Nayak, A. Saxena, Phys. Rev. C 95 (2017) 024619.
[16] H. Rameback, et al., J. Radioanal. Nucl. Chem. 304 (1) (2015) 467–471.
[17] T. Vidmar, G. Kanisch, G. Vidmar, Appl. Radiat. Isot. 908 (2011) 69.
[18] R. Pachuau, et al., Nucl. Phys. A 992 (2019) 121613.
[19] D.L. Smith, N. Otuka, Nucl. Data Sheets 113 (12) (2012) 3006–3053.
[20] B. Lawriniang, et al., J. Radioanal. Nucl. Chem. 319 (3) (2019) 695–701.
[21] A. Gandhi, et al., Eur. Phys. J. Plus 136 (8) (2021) 819.
[22] N. Otuka, et al., Radiat. Phys. Chem. 140 (2017) 502–510.
[23] A. Gandhi, et al., Chin. Phys. C 46 (1) (2022) 014002.
[24] A. Gandhi, et al., Eur. Phys. J. A 57 (1) (2021) 1.
[25] A.J. Koning, D. Rochman, Nucl. Data Sheets 113 (2012) 2841.
[26] Mert Sekerci, Radiochim. Acta 108 (6) (2020) 459–467.
[27] A. Gilbert, A.G.W. Cameron, Can. J. Phys. 43 (1965) 1446.
[28] W. Dilg, W. Schantl, H. Vonach, M. Uhl, Nucl. Phys. A 217 (1973) 269.
[29] A.V. Ignatyuk, J.L. Weil, S. Raman, S. Kahane, Phys. Rev. C 47 (1993) 1504.
[30] S. Goriely, F. Tondeur, J.M. Pearson, A Hartree–Fock nuclear mass table, At. Data Nucl. Data Tables 77 (2) (2001) 311–381.
[31] S. Goriely, S. Hilaire, A.J. Koning, Phys. Rev. C 78 (2008) 064307.
[32] S. Hilaire, M. Girod, S. Goriely, A.J. Koning, Phys. Rev. C 86 (2012) 064317.
[33] A. Karpeles, Radiochim. Acta 12 (1969) 115–117.
[34] Y. Nagame, et al., Int. J. Appl. Radiat. Isot. 29 (1978) 615–619.
[35] M. Aikawa, M. Saito, S. Ebata, Y. Komori, H. Haba, Nucl. Instrum. Methods Phys. Res., Sect. B, Beam Interact. Mater. Atoms 427 (2018) 91–94.